EURASIP Journal on Applied Signal Processing 2004:12, 1886–1898

Design of Farthest-Point Masks for Image Halftoning

R. Shahidi
Electrical & Computer Engineering, Faculty of Engineering and Applied Science, Memorial University of Newfoundland, St. John's, NL, Canada A1B 3X5
Email: shahidi@engr.mun.ca

C. Moloney
Electrical & Computer Engineering, Faculty of Engineering and Applied Science, Memorial University of Newfoundland, St. John's, NL, Canada A1B 3X5
Email: cmoloney@engr.mun.ca

G. Ramponi
Image Processing Laboratory, DEEI, University of Trieste, 34127 Trieste, Italy
Email: ramponi@univ.trieste.it

Received 3 September 2003; Revised 5 January 2004

In an earlier paper, we briefly presented a new halftoning algorithm called farthest-point halftoning. In the present paper, this method is analyzed in detail, and a novel dispersion measure is defined to improve the simplicity and flexibility of the result. This new stochastic screen algorithm is loosely based on Kang's dispersed-dot ordered dither halftone array construction technique used as part of his microcluster halftoning method. Our new halftoning algorithm uses pixelwise measures of dispersion based on one proposed by Kang which is here modified to be more effective. In addition, our method exploits the concept of farthest-point sampling (FPS), introduced as a progressive irregular sampling method by Eldar et al. but uses a more efficient implementation of FPS in the construction of the dot profiles. The technique we propose is compared to other state-of-the-art dither-based halftoning methods in both qualitative and quantitative manners.

Keywords and phrases: image halftoning, ordered dither, irregular sampling, halftoning quality measures.

1. INTRODUCTION AND BACKGROUND

1.1. Introduction

Digital halftoning refers to transforming a many-toned image into a one with fewer tones, perhaps only two, for the purposes of either rendering or printing. In this paper, we consider only bi-level halftoning of gray-scale images using point-by-point comparison with a threshold array (ordered dither). Five techniques for doing this halftoning are now briefly described; the new farthest-point halftoning (FPH) algorithm presented in this paper is loosely based on the fifth, Kang's dispersed-dot ordered dither. This section is concluded by a comment on a method for irregular sampling, which is at the root of our method.

1.2. Ordered dither halftoning techniques

In this section, we review previous methods of ordered dither halftoning to which we compare our new FPH technique. We also review Kang's dispersed-dot ordered dither algorithm which is the basis for FPH.

1.2.1. The modified blue noise mask

The modified blue noise mask (MBNM) technique [1] starts by creating an initial pattern of "ink" dots using an algorithm called binary pattern power spectrum matching algorithm (BIPPSMA). This algorithm converts a white noise pattern at a given gray level g_i to a blue noise pattern at the same gray level. The initial white noise pattern is filtered with a level-dependent Gaussian in the frequency domain and then converted back to the spatial domain. The result is no longer binary, but the largest values of the filtered pattern where there was a 1 in the binary pattern correspond to the largest clusters of dots, while the smallest values of the filtered pattern where there used to be a 0 correspond to the largest voids (areas where dots are absent). So the highest M centres (where M is a parameter) of largest clusters and voids are swapped, and the mean squared error (MSE) of the new binary pattern with respect to the current gray level is computed. If the MSE goes down, the swapping process continues with the new pattern; otherwise, the process continues with $M/2$, unless M is 1, in which case the process has converged.

Once the initial binary pattern has been obtained, the main MBNM algorithm uses a BIPPSMA-like procedure. Only the upwards procedure is described here; the downwards progression is similar. It starts off with the initial binary pattern from the last level, and randomly converts U_k of the pixels from 0 to 1. Then, the same filtering operation is performed, but when looking for the M 0's and 1's to swap, only the 1's that are in the current binary pattern, but were not in the pattern from the next lowest level, are considered. The convergence criterion is the same as for BIPPSMA.

The gray-level dependent Gaussian filter is of the form $F(u,v) = e^{-r^2/2\sigma^2}$, where $r^2 = u^2 + v^2$ and u and v are frequency coordinates. $\sigma = 0.4 f_g$, where $f_g = \min(\sqrt{g}, \sqrt{1-g})$.

1.2.2. The void-and-cluster method

The void-and-cluster method (VAC) [2] tries to eliminate unwanted clumps and empty regions (i.e., without 1's) in the halftone threshold array and thus in the halftoned image itself. Like the MBNM, the VAC algorithm starts with an initial binary pattern at an intermediate gray level g_i. This is created via the initial binary pattern generator, which starts off with an arbitrary pattern with a fraction g_i of pixels turned on. Then clusters (groups of "on" pixels) and voids (areas without any "on" pixels) are iteratively reduced. These clusters and voids are found by computing a circular convolution of the binary pattern $b(x, y)$ with a Gaussian filter, like the one used in MBNM. A good value of σ was found to be 1.5 [2].

A circular convolution is used in order to allow smaller halftone arrays to be generated which can be tiled over a larger image. The minimum of the convolution can be viewed as being the centre of the largest void, while the maximum can be regarded as the centre of the tightest cluster. In the initial binary pattern generator, the centre of the tightest cluster and the centre of the largest void are swapped. This process is ended when there is no change in the current iteration, so the process is converged.

The rest of the VAC algorithm is straightforward. First, the dot profiles for all gray levels greater than g_i are built, and then those for levels less than g_i are built, by turning on the centres of the largest voids in the upwards progression and turning off the centres of the largest clusters when going down.

1.2.3. Direct binary search screen

In the traditional direct binary search (DBS) method, a human visual model is used to minimize the energy of the error between the original gray-scale image and its halftone. This has to be done for each image to be halftoned and is therefore computationally very expensive. The DBS screen method was originated in [3] by Allebach and Lin, with refinements in [4, 5], avoiding the burden of using the DBS algorithm for each image, by creating a single dither matrix.

The DBS screen method starts from a random pattern at a given gray level, then refines it via a metric which is based on a lowpass filtered version of luminance (L^*), representing in turn the frequency response of the human visual system (HVS). The filter is governed by a parameter which is a function of the gray level. In the pattern, pixel swapping is used to reach the minimum value for the metric. Once the dot profile of the initial gray level is designed, dot profiles for lighter and darker gray levels are designed in a similar manner: at each step, a random selection of pixels is added to or deleted from the pattern, satisfying the stacking property; then, the metric is again minimized.

The authors mention in [3] that halftoning with the DBS screen shows some advantages but also drawbacks with respect to the VAC method. In private communication with S. H. Kim, he has stated that the dual-metric DBS in a paper he coauthored with Allebach [6] is an improved version of regular DBS [3] since it uses a tone-dependent HVS model as opposed to a fixed one. This visual system model is a two-component Gaussian in frequency based on a model by Näsänen. We therefore use the dual-metric DBS method of [6] (which we hereafter refer to with the abbreviation DBS) for comparison with our FPH algorithm.

1.2.4. Linear pixel shuffling halftoning

Linear pixel shuffling (LPS) was introduced in [7] as a way to index a 2-dimensional array; it uses a Fibonacci-like sequence so that indices close to each other point to elements far apart in the array. The halftoning algorithm based on LPS constructs the dot profiles upwards by turning on the pixels in the LPS order, and then summing and inverting to create the halftone mask.

To be precise, let $G_0 = 0$, $G_1 = G_2 = 1$, $G_k = G_{k-1} + G_{k-3}$ for $k > 2$, and $G_{k-3} = G_k - G_{k-1}$ for $k \leq 2$. Let the matrix $M = \begin{pmatrix} G_{-n+1} & G_{n-3} \\ G_{-n} & G_{n-2} \end{pmatrix}$. Then we start with all the pixels "off" or 0, and go through the image in raster-scan order. Say we are at index (i, j) in this raster scan. Then at this step, we turn the pixel $M * (i, j)^T$ on, where $*$ denotes matrix multiplication and T is the transpose operator. When enough pixels have been turned on in the current level from the previous level, the level number is incremented.

1.2.5. Kang's dispersed-dot ordered dither algorithm

Kang outlines an algorithm in [8] for creating dispersed-dot ordered dither arrays of arbitrary dimensions. Kang's algorithm is used for microcluster halftoning, a cross between dispersed-dot and clustered-dot ordered dither. In his application, only very small (e.g., 5×5) masks need to be formed.

Thus, efficiency was not a concern for Kang. In fact, in the description of his mask formation algorithm in [8], it appears that Kang performs a brute-force search through all the unselected pixels in the image. His algorithm generates the dot profiles of the threshold array in an upwards fashion, starting at level 0 with an all-zero mask; at each stage, it chooses the pixel which is the most dispersed with respect to all the pixels previously turned on (or to a 1). Whereas in LPS [7], pixels can be visited in the order of their indices in a table, Kang's algorithm chooses the next pixel to be the one with the smallest calculated *dispersion*. This dispersion is a function of the distances to the four closest pixels which are already 1's; this would be computationally inefficient for larger masks due to the fact that the four nearest neighbors

would have to be recalculated for all pixels after a new pixel is turned on. Our approach, based on a generalization of farthest-point Sampling (FPS) in [9], can solve this problem very quickly, as we discuss in Section 2.

Kang defined the dispersion of a pixel to be

$$\Lambda(i,j) = \sum_{k=1}^{4} \frac{|\, d_k(i,j) - \bar{d}(i,j)\,|}{\bar{d}(i,j)}, \tag{1}$$

where $\bar{d}(i,j)$ is the average distance to the four nearest neighbors of pixel (i,j) and $d_k(i,j)$ is the distance to the kth closest neighbour of this pixel in the image I. This tends to be low for positions which are far away from "on" pixels and where the variance of the distances to pixels already turned on is small. Unfortunately, the dispersion measure does not distinguish between pixels which are equidistant from their four nearest neighbors, since regardless of this distance, the dispersion is 0. For example, if the four nearest neighbors of two different pixels are at distances of $(1,1,1,1)$ and $(4,4,4,4)$, respectively, they are treated identically. This is not a major issue with the formation of small halftone masks but becomes more important when creating larger halftone masks as we wish to do in this paper.

Kang's algorithm sequentially selects pixels with the lowest dispersion until there are only single-pixel "holes," for which the four immediately adjacent horizontal and vertical positions are on. Then, the holes which are closest to the other holes and with the smallest dispersion are selected. The problem with this approach is that even before all the remaining pixels to be filled are holes, there are many ties, as many candidate pixels have the same four closest distances. In effect, for higher gray levels, the dispersion contains less information about the best pixel to choose next.

1.3. Towards farthest-point halftoning

In a different context, the FPS method, using an incremental Voronoi diagram construction process, was introduced in [9] for effective irregular sampling of an image. To exploit it for halftoning, the key observation is that in general, a good set of irregular samples will have a blue noise spectrum, which is the desired characteristic of the spectra of good dot profiles for halftoning [10]. An irregular sampling method applied to halftoning might start from the dot profile for gray level 0 and work its way up, at each point choosing the next pixel to be the one that is the farthest from all previously selected pixels. This idea is not practical however, because of the extreme amount of time needed to sample the entire image for the formation of all the dot profiles of all gray levels.

In this paper, we introduce our new FPH algorithm, and we compare its performance to those of existing algorithms: the MBNM [1], the VAC method [2], the dual-metric DBS method [6], and halftoning with an LPS threshold array [7].

2. FARTHEST-POINT HALFTONING

Given a gray-scale image I, we use the previously defined $d_k(i,j)$ with a Euclidean norm. Then, a faster version of the FPS method in [9] can be used to update the four nearest neighbors of each pixel. At each stage, FPS chooses the pixel which is the farthest away from all previously selected pixels using a Voronoi diagram. However, our speed-up is achieved because of the fact that only distances between points on the integer lattice need to be computed in the context of halftoning, meaning that a lookup table can be utilized to find these distances. Also in the image I, the update of the four nearest neighbours is a local process because only pixels which are within $\max_{(i,j)\in I} d_4(i,j)$ of the pixel just changed to 1 or 0 need to have their d_i values updated.

Using FPS, it is hard to find the closest C "on" pixels to every "off" pixel in the image, where C is an integer constant greater than 1, but this is easily handled with our variant, where C is taken to equal 4. Therefore, it is possible to generate reasonably sized dither arrays, for example, 128×128 (which can be tiled for use with larger images with a toroidal topology), in about the same time as or faster than the existing MBNM and VAC algorithms. More specifically, it was found that the creation of a 128×128 FPH mask took only 6.85 seconds on a computer with an AMD Athlon XP 1700+ Processor with 256 MB RAM, and the construction of a 256×256 FPH mask required 40.93 seconds on the same system. Due to different implementations of halftone mask generation for the FPH, VAC, MBNM, and LPS algorithms, they were not precisely comparable, but were experimentally observed to have running times of the same order of magnitude. DBS is computationally more expensive.

2.1. New dispersion measures

In this section, we present two ways to improve Kang's dispersion measure for use in our FPH algorithm.

2.1.1. New dispersion measure Λ_1

Due to the problems with Kang's dispersion measure, we proposed a new dispersion measure Λ_1 in [11]:

$$\begin{aligned}\Lambda_1(i,j) = {} & w_1\Lambda(i,j) + w_2 \sum_{k=1}^{4} e^{-d_k^2(i,j)/2\sigma^2} + \frac{w_3}{d_4(i,j)} \\ & + w_4 cb(i,j) + w_5 o(i,j) + w_6\Delta(i,j).\end{aligned} \tag{2}$$

The coefficients $\{w_i\}_{i=1}^{6}$ of the terms in the above equation are constants; we recommend good values for these weights in Section 2.1.3. Each of the six components of (2) has a precise role in describing dispersion for use in our proposed dot profile formation process, which is described in detail in Section 2.2. We note here that in our dot profile formation process, pixels can be turned both on and off, unlike in Kang's algorithm in which pixels are only turned on.

The function $\Lambda(i,j)$ in the first term of (2) is Kang's dispersion measure from (1); it ensures that the pixels being turned on or off are not too unbalanced with respect to pixels which are already on or off, respectively. The exponential components of the second term are meant to keep these pixels far apart. The purpose of the $1/d_4(i,j)$ and $cb(i,j)$ terms is to reduce the appearance of checkerboard patterns in the dot profiles. The $1/d_4(i,j)$ term is used to suppress checkerboard

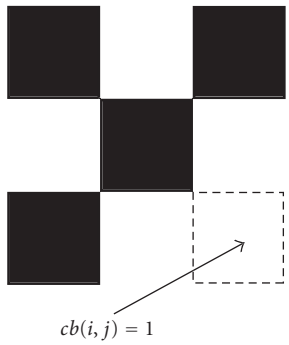

Figure 1: Example of a pixel forming a local checkerboard pattern.

patterns because it is high when switching a pixel on or off with all closest neighbors $\sqrt{2}$ away. However, this does not prevent the formation of checkerboards by turning on or off pixels in other parts (not the centre) of the texture. This is why a *cb* term is also used, and we describe it in more detail below. Finally, the $o(i, j)$ and $\Delta(i, j)$ terms avoid horizontal, vertical, or diagonal arrangements of dots.

The functions in the last three terms of (2) are defined by the following expressions:

$$cb(i,j) = \begin{cases} 1 & \text{if turning } (i,j) \text{ on (or off)} \\ & \text{forms a checkerboard,} \\ 0 & \text{otherwise,} \end{cases}$$

$$o(i,j) = \begin{cases} 1 & \text{if } d_1(i,j) = 1, \\ 0 & \text{otherwise,} \end{cases} \tag{3}$$

$$\Delta(i,j) = \begin{cases} 1 & \text{if } d_1(i,j) = \sqrt{2}, \\ 0 & \text{otherwise.} \end{cases}$$

The term $cb(i, j)$ is set to 1 if turning pixel (i, j) on or off forms a checkerboard pattern with respect to the pixels which are already on or off, respectively. Were the checkerboard suppression term $cb(i, j)$ not included, the dispersion of the pixels forming the checkerboard term would be too low, and the formation of checkerboard patterns not brought into existence by turning on the middle pixel would be favored at levels far away from the middle level. The middle levels are where these patterns are better tolerated. Figure 1 shows an example of a pixel whose *cb* value is 1. When turning a pixel on or off, we also must check whether some pixels which before had $cb(i, j) = 1$ have now changed to have $cb(i, j) = 0$ and vice versa.

However, if we penalize checkerboard patterns, then horizontal and vertical arrangements also become too highly favoured. So we add a penalty term $o(i, j)$ for the formation of these arrangements, which can be easily identified by checking whether the closest distance to a pixel with the same binary value is 1. We do the same for diagonal configurations (with $\Delta(i, j)$) by penalizing arrangements with closest distance equal to $\sqrt{2}$. This type of control of texture is akin to the texture enhancement/suppression in halftones found in the paper by Scheermesser and Bryngdahl [12].

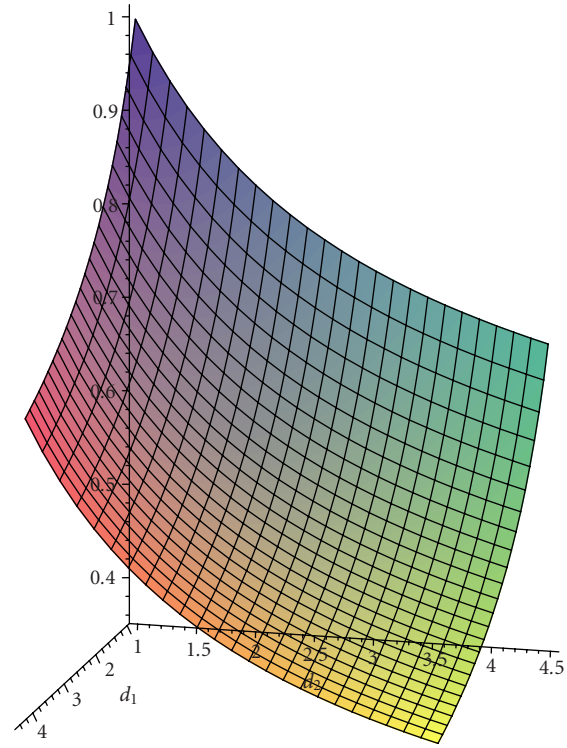

Figure 2: Plot of simplified dispersion term for two distances.

The exponential terms used in the computation of Λ_1 are similar to the Gaussian filter in the VAC method [2]. The exponential terms are present so that positions which are close to already switched pixels (with $\{d_i\}_{i=1}^4$ small) are less likely to be chosen than those which are far. So, for instance, if we use the same example as in Section 1.2.5, now two pixels with respective closest distances $(1, 1, 1, 1)$ and $(4, 4, 4, 4)$ will have distinct dispersions, the one with all closest distances equal to 1 with the higher dispersion.

2.1.2. *New dispersion measure* Λ_2

Although the dispersion measure Λ_1 proposed above and in [11] is effective, it is quite complex. Also, it has been found that there is a large dependence of the dispersion coefficients on the size of the mask being generated. A new dispersion measure Λ_2 is now proposed to deal with these two disadvantages of Λ_1. The expression for Λ_2 is as follows:

$$\Lambda_2(i,j) = \sum_{k=1}^{4} \frac{w_{1,k}}{1 + d_k^2(i,j)} + w_2 o(i,j) + w_3 cb(i,j), \tag{4}$$

where $o(i, j)$ and $cb(i, j)$ are as defined for Λ_1. The $w_{1,k}$'s are weights which are included because the distances to the four closest on or off pixels will rarely all be exactly equal, but there will be some inbalance between them, even if not very significant. This will be more clear after the argument justifying the use of Λ_2. The $\sum_{k=1}^{4}(w_{1,k}/(1+d_k^2(i,j)))$ term is smaller for larger values of the d_k's as well as when the d_k's are close in value to each other. The function $1/(1 + d_1^2) + 1/(1 + d_2^2)$

is plotted in Figure 2 and clearly possesses these two desired characteristics.

Thus, this term has the properties required to absorb Kang's dispersion measure Λ and the VAC-like exponential terms in Λ_1. We can show that equal or roughly equal values of the d_k's are favoured by an argument using the arithmetic mean-harmonic mean (AM-HM) inequality. By the AM-HM inequality,

$$\begin{aligned}\frac{4}{\sum_{k=1}^{4}\left(1/\left(1+d_k^2(i,j)\right)\right)} &\le \frac{1}{4}\sum_{k=1}^{4}\left(1+d_k^2(i,j)\right)\\ &= 1+\frac{1}{4}\sum_{k=1}^{4}d_k^2(i,j)\end{aligned} \tag{5}$$

with equality when the $d_k(i,j)$'s are all equal to each other. In other words, if $1+(1/4)\sum_{k=1}^{4}d_k^2(i,j) = c$, where c is some constant, then $\sum_{k=1}^{4}(1/(1+d_k^2(i,j)))$ is minimal when all the $d_k(i,j)$'s are equal (this can be obtained by taking the reciprocal of each side of the inequality). Similarly, $\sum_{k=1}^{4}(w_{1,k}/(1+d_k^2(i,j)))$ is minimal for $d_k(i,j)$'s with $\sum_{k=1}^{4}((1+d_k^2(i,j))/w_{1,k}) = c$, with c a constant, when all the $d_k^2(i,j)/w_{1,k}$'s are equal. So this is where the $w_{1,k}$ weights come into play.

Further, it is possible, using an argument based on Lagrange multipliers, to show that the term $\sum_{k=1}^{4}(1/(1+d_k^2(i,j)))$ for $\sum_{k=1}^{4}d_k = c$, where c is a given constant, is minimized when all the $d_k(i,j)$'s are equal. The simple proof is omitted here, but uses the fact that $d_k \ge 1$ for all k, and that for such d_k, $d_k/(d_k^2+1)^2$ is monotonic.

2.1.3. Setting the weights

The weights w_i used in the expression for Λ_1 in (2) should be selected as a function of the size of the dot mask; for example, in all our experiments with 128×128 grids, a convenient choice was $\mathbf{w} = [0.6, 1.7, 1.0, 0.65, 1.2, 0.8]$, slightly different than those in [11]. The parameter σ was also experimentally selected to be 1.5. The setting of these parameters is critical to good halftoning; we have established the above values to work well for 128×128 halftone masks (which can be tiled to create larger masks) across a variety of images.

For Λ_1, the weights that worked for the 128×128 mask size would not work for the larger 256×256 size. This mask-size sensitivity is discussed further in Section 4.1.2.

Suitable values for the weights for Λ_2 in (4) were found to be $\mathbf{w}_1 = [4.8, 5.2, 6.0, 6.4]$, $w_2 = w_3 = 0.8$ for a 256×256 halftone mask. Unlike Λ_1, the performance of which was significantly degraded when the mask size was changed, the loss in halftone quality was quite small when the Λ_2 mask was changed to a size of 128×128 pixels from 256×256 pixels with the same parameters.

2.2. Formation of dot profiles

In this section, we show how the dispersion measures of Section 2.1 are used to create dot profiles for FPH.

Suppose that the original image has luminance range $[0, G-1]$. In Kang's method, the dot profiles are generated by starting at gray level 0, and successively generating the dot profiles at the next gray level higher until we get to the dot profile of the highest gray level. Because of the problems with a strictly upward progression in Kang's method, previously discussed in Section 1.2.5, a two-step procedure around an intermediate level g is used to create the dot profiles. If $g = \lfloor G/2 \rfloor$, as we recommend, then dispersions are always taken with respect to minority pixels. The two-step process we propose is as follows.

(1) Create the dot profiles for all levels up to and including an intermediate level g, starting from level 0, picking the pixel with the lowest dispersion at each stage. Start off with four randomly pixels turned on.

(2) Build the dot profiles from level $G-1$ down to level $g+1$. Note that the dot profiles must satisfy a stacking constraint, that is, if a pixel is on in one level, it has to be on for all higher levels. So whenever a pixel is turned off, it must be already off in the dot profile for level g. The downward process starts with an initial pattern for level $G-1$ with all pixels on except for four random pixels chosen from those which are off at level g. Then pixels are turned off which have the lowest dispersions (Λ_1 or Λ_2) with respect to off pixels. When enough pixels have been turned off in a level ($\sim mn/G$ for an $m \times n$ image), the level is decremented and so on until the dot profile for level $g+1$ is formed.

Finally all the individual dot profiles are summed to produce the threshold array against which an input gray-level image is compared for halftoning. We give the name of FPH to the entire process, that is, the threshold array generation followed by the actual halftoning.

3. EVALUATION OF HALFTONE QUALITY

In this section, we briefly list and describe the halftone quality measures and analysis tools which we use to compare FPH with the existing algorithms. These are the measures found in the halftoning toolbox for Matlab [13], Wong's mixture distortion criterion [14] based on the frequency-weighted MSE (FWMSE), and morphological characterization of halftone masks [15].

3.1. Halftone quality measures

3.1.1. Halftoning toolbox for Matlab

The halftoning toolbox for Matlab [13] includes implementations of four quantitative measures of halftone quality. We use these to compare halftones generated from the previous algorithms with our own FPH. These measures are weighted SNR (WSNR), peak SNR (PSNR), the linear distortion measure (LDM) and the image quality index (IQI). The lower the LDM, the better the halftone, while for the other three measures, halftone quality becomes greater with increasing measure value. More details on these measures may be found in the source code documentation of the halftoning toolbox for Matlab [13].

3.1.2. Frequency weighted mean square error

The FWMSE measures the distortion of a halftone from the original image as viewed by a human observer. There are two versions of the FWMSE, both using a model of the human

visual system (HVS). The first version measures the difference between the original image and the halftoned image, both as viewed using the HVS, whereas the second measures the difference between the original image and the halftoned image, where only the halftone is viewed by the HVS. We use the first version where both the original and halftoned image are filtered with the frequency response of the modified Mannos-Sakrison visual model [14].

The FWMSE on its own has problems; it is possible for a less uniform halftoned image of a constant gray patch to have a lower FWMSE than one which is more uniform. So Wong [14] proposed a mixture distortion criterion for halftones, where there is an additional penalty added to the FWMSE if two minority pixels are closer than the principal distance ($\min(1/\sqrt{g}, 1/\sqrt{1-g})$ for gray level g) or if we wish to add a majority pixel instead of a minority pixel at a distance further away than this principal distance from the nearest minority pixel.

Wong's mixture distortion criterion only measures the quality of a halftone of a constant gray-level image. To compare two halftoning algorithms, we follow the approach of Yao [16] and measure the halftone quality of constant gray-level images halftoned with the masks from the two algorithms at every eight gray levels. The results are found in Section 4.1.3.

3.2. Morphological characterization

Misic and Parker [15] proposed a mechanism of analysing and comparing halftone masks using a small window sliding across the dot profiles of the mask. Configurations of white and black pixels in this window, which was 2×2 pixels for the example masks given in their paper, are counted for the dot profiles at each of the gray levels, and then plotted against and compared to each other.

One preferred characteristic of the distributions of patterns is that the number of diagonal configurations should always be greater than the number of horizontal and vertical ones at a given gray level. As an example, in [15], two hypothetical masks are compared, one with more combined horizontal and vertical patterns than diagonal patterns, and one with the reverse holding. They state that the one with more diagonal configurations is better.

We compare the morphological characterizations of FPH against VAC and DBS in Section 4.1.

4. RESULTS AND DISCUSSION

4.1. Results

4.1.1. Halftoned image results

Original test images

All test images are 256×256 pixels large, including a ramp image with luminance range $[0, 255]$ defined as having intensity $R(i, j) = i$, $0 \le i \le 255$, at the pixel on the ith row and jth column of the image. The *ramp* image was used in our tests since it clearly contains all different gray levels, and thus problems in halftoning any specific gray level can be detected. Two original grayscale test images, *peppers* and *femme*, are shown in Figure 3.

(a) (b)

Figure 3: (a) Original 256 tone, 256×256 peppers image and (b) original 256 tone, 256×256 femme image.

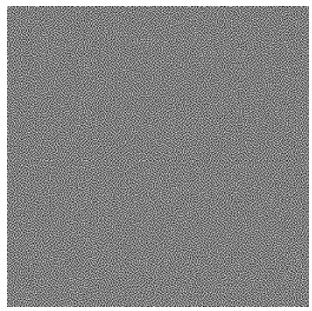

Figure 4: 256×256 halftone mask using FPH with dispersion measure Λ_2.

FPH mask and halftones

We give a concrete example of a halftone mask generated by FPH in Figure 4. This figure shows a 256×256 halftone mask using our FPH algorithm with dispersion measure Λ_2. Observe the lack of clumps suggesting the presence of the blue noise characteristic desired for halftone threshold arrays.

Figure 5 gives the results of peppers halftoned with the MBNM, VAC, DBS, LPS, and FPH methods (including both the Λ_1 and Λ_2 versions of FPH) with 128×128 mask sizes. Figure 6 compares the halftones of the peppers image for these methods with a mask size of 256×256 pixels, where only Λ_2 is used with FPH.

Similarly, Figure 7 presents the halftones of the femme image from all algorithms obtained with 128×128 masks, while Figure 8 gives the halftones of femme from the algorithms with 256×256 masks, with only the second dispersion measure Λ_2 being used for the FPH mask.

Finally, Figure 9 shows the results of the ramp image halftoned with the MBNM, VAC, DBS, LPS, and both FPH methods with 128×128 mask sizes. Figure 10 compares the halftones of ramp for these techniques with a 256×256 mask size, with only Λ_2 being used for FPH.

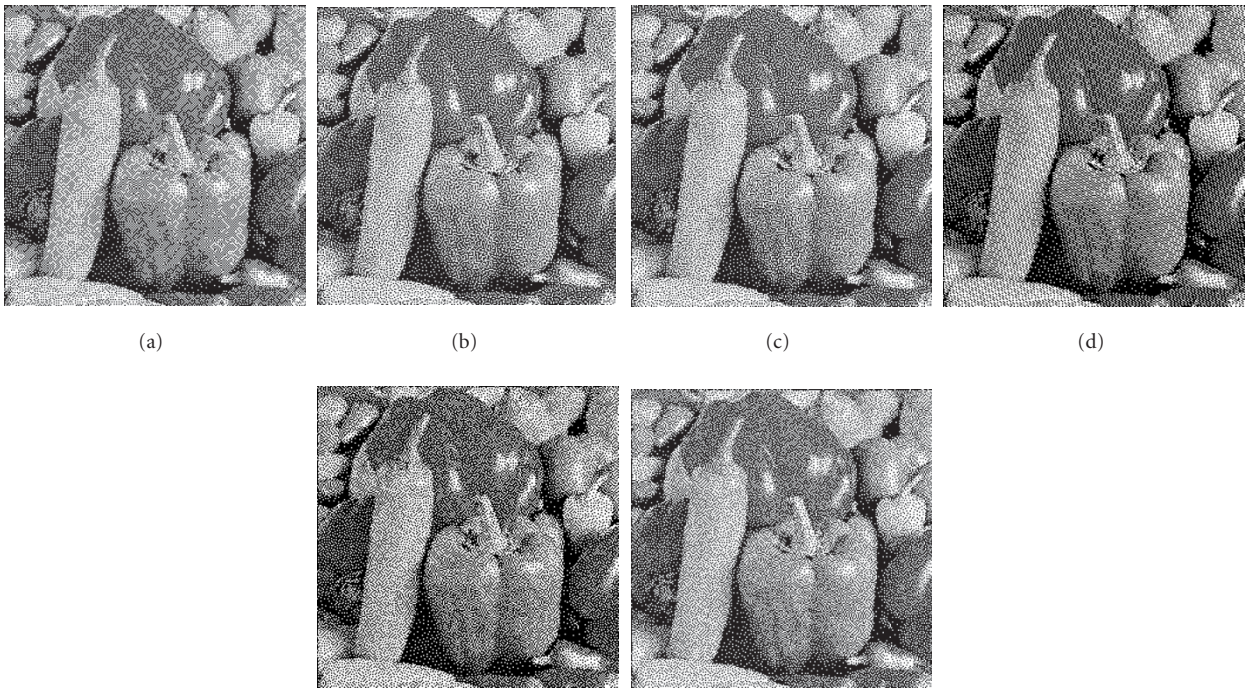

(a) (b) (c) (d)

(e) (f)

Figure 5: Peppers halftoned with (a) tiled 128×128 MBNM, (b) tiled 128×128 VAC mask, (c) tiled 128×128 DBS mask, (d) tiled 128×128 LPS mask, (e) tiled 128×128 FPH mask (Λ_1), and (f) tiled 128×128 FPH mask (Λ_2).

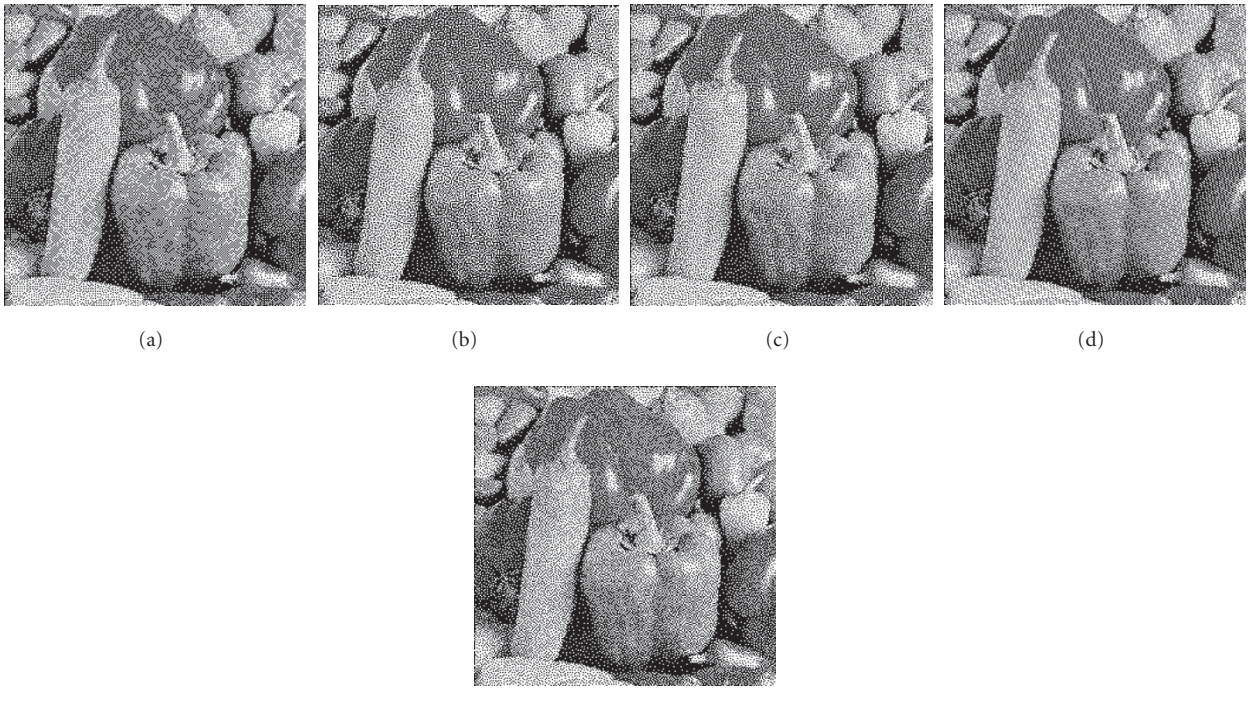

(a) (b) (c) (d)

(e)

Figure 6: Peppers halftoned with (a) 256×256 MBNM, (b) 256×256 VAC mask, (c) 256×256 DBS mask, (d) 256×256 LPS mask, and (e) 256×256 FPH mask (Λ_2).

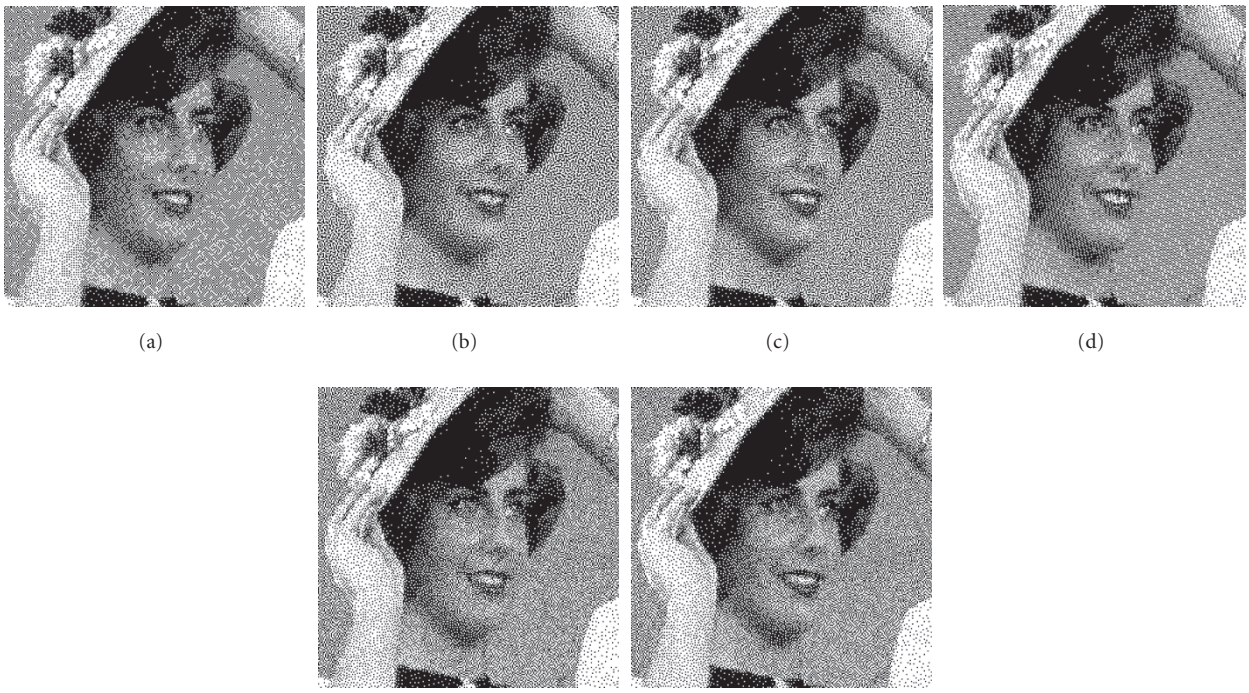

(a) (b) (c) (d)

(e) (f)

Figure 7: Femme halftoned with (a) tiled 128×128 MBNM, (b) tiled 128×128 VAC mask, (c) tiled 128×128 DBS mask, (d) tiled 128×128 LPS mask, (e) tiled 128×128 FPH mask (Λ_1), and (f) tiled 128×128 FPH mask (Λ_2).

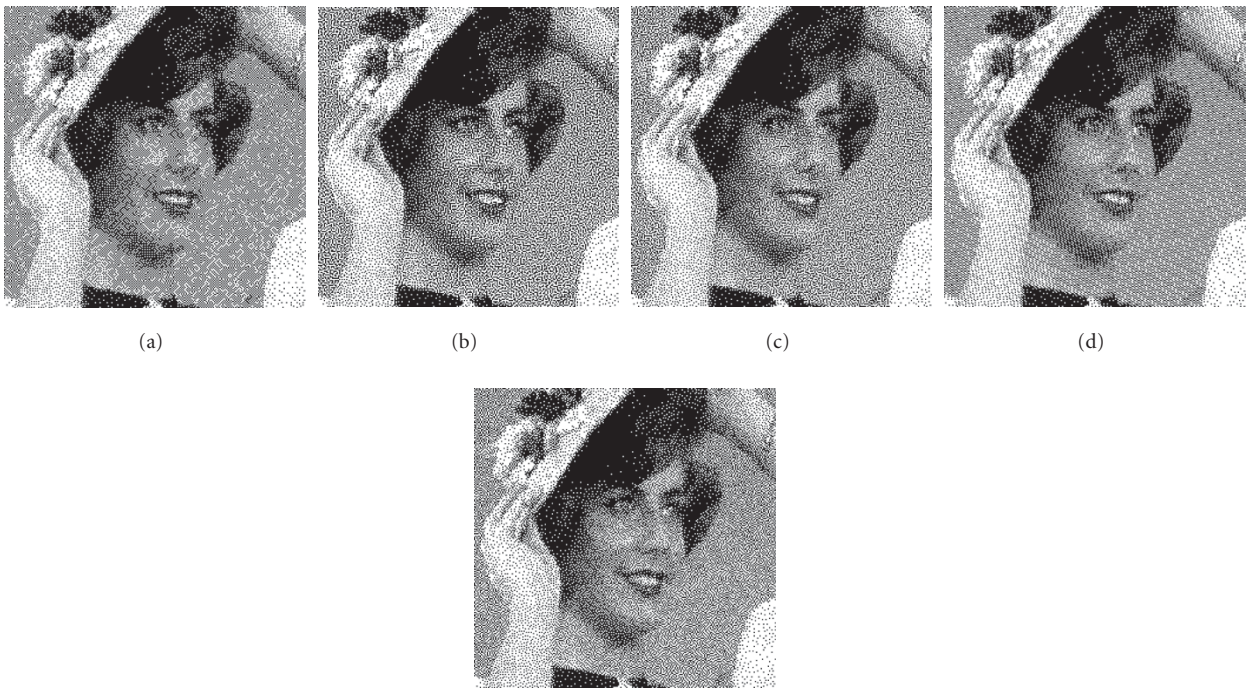

(a) (b) (c) (d)

(e)

Figure 8: Femme halftoned with (a) 256×256 MBNM, (b) 256×256 VAC mask, (c) 256×256 DBS mask, (d) 256×256 LPS mask, and (e) 256×256 FPH mask (Λ_2).

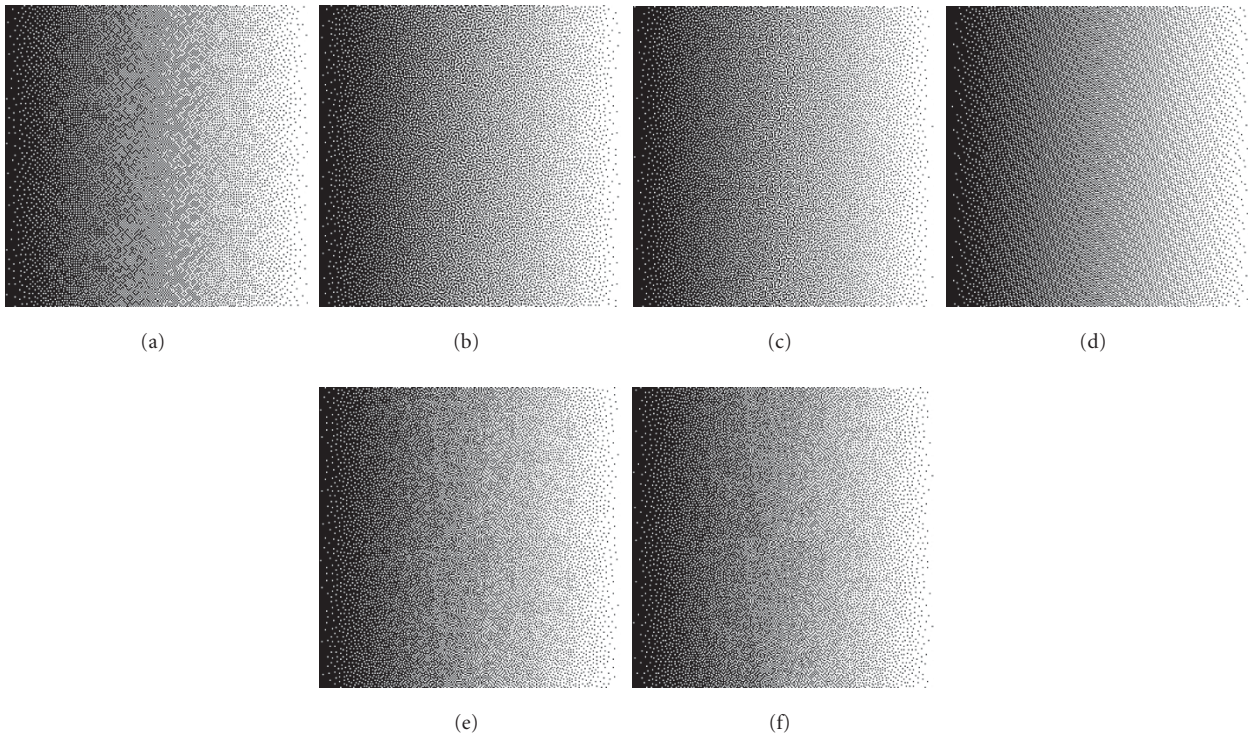

FIGURE 9: Ramp halftoned with (a) tiled 128×128 MBNM, (b) tiled 128×128 VAC mask, (c) tiled 128×128 DBS mask, (d) tiled 128×128 LPS mask, (e) tiled 128×128 FPH mask (Λ_1), and (f) tiled 128×128 FPH mask (Λ_2).

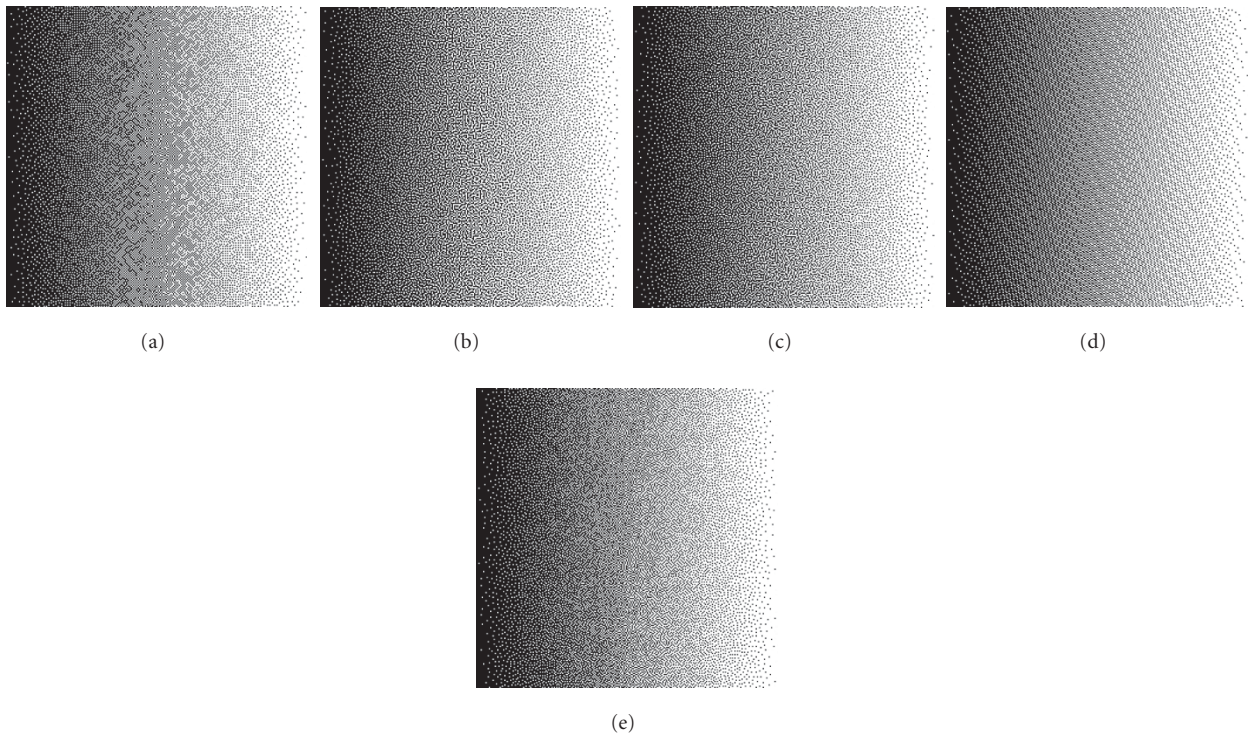

FIGURE 10: Ramp halftoned with (a) 256×256 MBNM, (b) 256×256 VAC mask, (c) 256×256 DBS mask, (d) 256×256 LPS mask, and (e) 256×256 FPH mask (Λ_2).

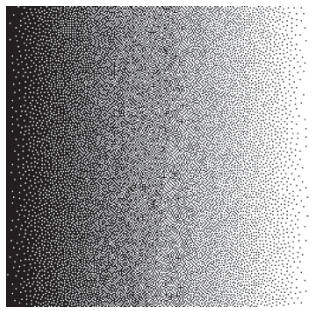

Figure 11: Using the same weights as for the 128×128 halftone mask (Λ_1) for the 256×256 FPH halftone mask.

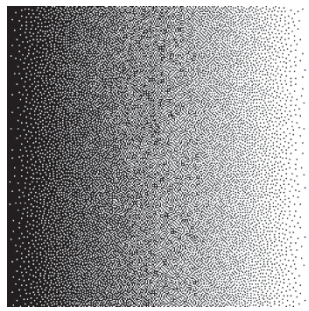

Figure 12: Lowering the horizontal/vertical weight penalty for the 256×256 FPH halftone mask (Λ_2).

Observe that we have included the tiled 128×128 LPS mask, even though it is not designed to be tileable. However, the additional error in all the measures is small because the tiling error is localized only to the boundaries of the tiled 128×128 masks.

4.1.2. Significance of weights

For halftoning with FPH, the parameters for the respective dispersion measures in Section 2.1.3 were used. As was stated earlier, the setting of these parameters is important for producing high-quality halftones using FPH.

An example of using the 128×128 mask weights for a 256×256 mask is shown in Figure 11 for the ramp image, where it can be seen that clusters of minority pixels are apparent, and there is less continuity between levels.

Although the same number of weights need to be set for the two dispersion measures, the expression for Λ_2 is simpler in form, and less of a balancing act is needed to select the parameters. The quality of results is however still sensitive to the choice of weights. The ramp image, halftoned using a 256×256 FPH mask, dispersion measure Λ_2, with the same weights as above, except for w_2 set to 0.2 instead of 0.8, is shown in Figure 12. As expected, there are more horizontal/vertical textures in the halftone, especially close to the midtones, than in the corresponding FPH halftone with proper weights ($w_2 = 0.8$) in Figure 10.

4.1.3. Halftone measure results

The halftone quality measures in the halftoning toolbox for Matlab for three test images (ramp, peppers, and femme) are tabulated in Tables 1, 2, and 3.

The mixture distortion criterion plots for the 128×128 masks are shown in Figure 13 and for the 256×256 masks in Figure 14. The morphological characterizations comparing the average number of occurrences of 2×2 diagonal patterns versus the average number of such horizontal/vertical patterns for the 256×256 masks of the FPH algorithm (Λ_2) and the VAC and DBS algorithms are shown in Figure 15.

4.2. Discussion

As anticipated, the halftones generated by the 256×256 masks are slightly better than those from the 128×128 masks. For the 128×128 masks, the VAC halftones (which have some coral-like patterns), the DBS halftones (with some noticeable horizontal/vertical patterns at midtones), and the FPH halftones from dispersion measure Λ_2 (with some diagonal artifacts) are the best in visual quality, followed by the FPH halftones from dispersion measure Λ_1 (which have some clustering for the mid-dark gray levels), the MBNM halftones (which have some alternating black and white checkerboard patterns), and the LPS halftones (with an obvious texture). The same qualitative ranking holds for the 256×256 masks with the same patterns, except for the absence of the FPH halftone with dispersion measure Λ_1. FPH has also been tested on a wide variety of other images, with consistent results.

From Tables 1, 2 and 3, we see that all the halftoning algorithms give similar values for the four measures, excluding the WSNR measures of the VAC and DBS algorithms. This, along with the qualitative assessment of the halftones, leads us to believe that the main competitors of FPH among existing halftoning algorithms are VAC and DBS. However, Figures 13 and 14 show that the FWMSE of the VAC mask at the midtones is much higher than the other algorithms, including FPH, and that the FWMSE of the DBS mask is also substantially higher than that of FPH at midtones. This is because checkerboard patterns are optimal at midtones close to gray level $g = 0.5$, explained by the fact that the HVS is more sensitive to horizontal/vertical patterns as opposed to diagonal ones, and any non-checkerboard patterns at these midtones necessarily must include horizontal/vertical arrangements of minority pixels. It should be mentioned however that the FWMSE of the DBS is somewhat penalized due to the fact that the model of the HVS used for the measurement of the FWMSE is different than that used for the calculation of the DBS screen.

As shown in Figure 15, the difference between the number of diagonal patterns and horizontal/vertical patterns is greater for the FPH algorithm (with dispersion measure Λ_2) as compared to the VAC and DBS algorithms, especially at midtones. This shows the superiority of our FPH halftoning method over the VAC and DBS algorithms at these middle gray levels.

Table 1: Halftone quality measures for ramp image.

Mask size	Algorithm	IQI ($\times 10^{-3}$)	LDM	PSNR	WSNR
128×128	MBNM	1.33	0.732	7.79	25.4
	VAC	1.37	0.744	7.78	28.2
	DBS	1.51	0.742	7.80	28.5
	LPS	1.39	0.766	7.78	26.9
	FPH(Λ_1)	1.39	0.737	7.77	25.5
	FPH(Λ_2)	1.41	0.750	7.78	25.9
256×256	MBNM	1.39	0.743	7.79	25.2
	VAC	1.34	0.745	7.78	28.2
	DBS	1.44	0.743	7.80	28.5
	LPS	1.34	0.740	7.78	27.4
	FPH(Λ_2)	1.39	0.745	7.79	25.8

Table 2: Halftone quality measures for peppers image.

Mask size	Algorithm	IQI ($\times 10^{-2}$)	LDM	PSNR	WSNR
128×128	MBNM	7.96	0.940	6.90	22.3
	VAC	7.78	0.940	6.88	24.3
	DBS	7.93	0.940	6.90	24.2
	LPS	7.98	0.942	6.90	23.6
	FPH(Λ_1)	7.96	0.940	6.90	22.9
	FPH(Λ_2)	7.85	0.940	6.90	23.2
256×256	MBNM	7.96	0.940	6.90	22.2
	VAC	7.93	0.940	6.89	24.3
	DBS	7.85	0.940	6.90	24.3
	LPS	7.98	0.940	6.90	24.0
	FPH(Λ_2)	7.83	0.940	6.89	23.1

Table 3: Halftone quality measures for femme image.

Mask size	Algorithm	IQI ($\times 10^{-2}$)	LDM	PSNR	WSNR
128×128	MBNM	6.94	0.935	7.42	23.8
	VAC	6.99	0.935	7.43	25.2
	DBS	6.95	0.935	7.43	25.1
	LPS	6.98	0.937	7.41	24.5
	FPH(Λ_1)	6.97	0.935	7.42	23.9
	FPH(Λ_2)	6.96	0.934	7.42	24.0
256×256	MBNM	6.89	0.935	7.42	23.7
	VAC	6.96	0.935	7.41	25.2
	DBS	7.01	0.935	7.42	25.1
	LPS	6.91	0.935	7.41	24.8
	FPH(Λ_2)	6.96	0.934	7.41	24.2

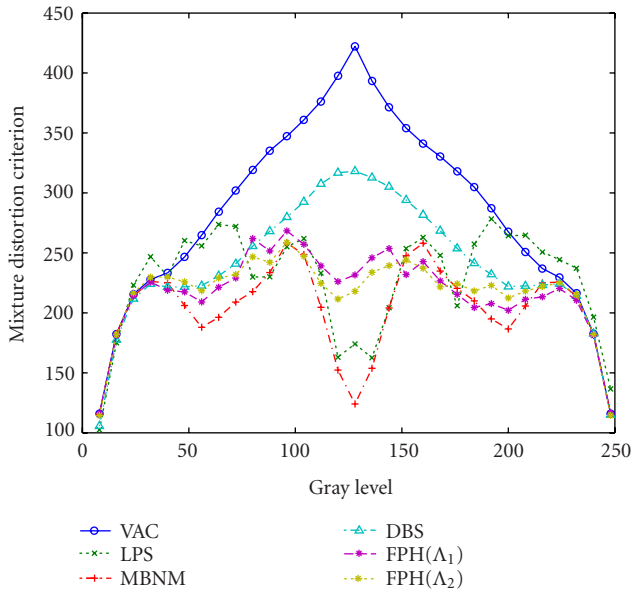

Figure 13: Mixture distortion criterion for 128×128 halftone masks from various algorithms.

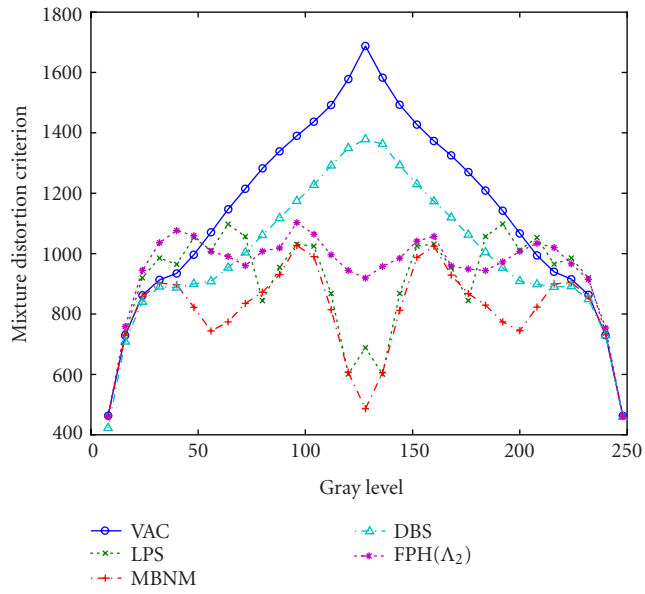

Figure 14: Mixture distortion criterion for 256×256 halftone masks from various algorithms.

While the halftone quality measures in Table 3 show the DBS halftones to be better than those of the FPH halftones, the differences are quite small. These two methods produce halftones of similar visual quality. The halftones from both methods contain minor artifacts, with each of DBS and FPH tending to produce slightly different artifacts. Additionally, as stated in Section 1.2.3, a dual-metric DBS algorithm is used to create the DBS halftones, with a tone-dependent HVS model. The weights in FPH do not depend on gray level, making FPH a less complex and more computationally efficient method, compared with dual-metric DBS.

5. CONCLUSIONS

In this paper, we have extended the FPH algorithm originally introduced in [11]. Its key points are the definition and exploitation of two novel dispersion measures which permit more visually pleasant distributions of the dot profiles; an upward/downward construction of the dot profiles themselves, which grants good uniformity of the dots at all gray levels; and a novel implementation of the FPS strategy which avoids the cumbersome creation of Voronoi diagrams and thus permits the rapid design of a halftoning mask.

The FPH results we obtain are visually good overall; apparent artificial structures and textures are not introduced in the halftone. FPH gives very good results, but there may be room for improvement. As already stated, the HVS is known to be less sensitive to diagonal configurations than horizontal and vertical ones. So for future work, this suggests the use of Manhattan instead of Euclidean distance. In addition, future study of the weight settings may result in weight settings which depend on the size of the halftone mask (for the first new dispersion measure Λ_1). Gray-level dependent weights can help in yielding halftones with a more uniform appearance over the gray-levels, and early results suggest that this may be a promising avenue to control the appearance of various patterns such as checkerboard and horizontal/vertical configurations in a more targeted manner, giving improved results. Finally, FPH could incorporate a human visual model as DBS does, or use morphological characterization to ensure that the frequency of any pattern is balanced with respect to any other.

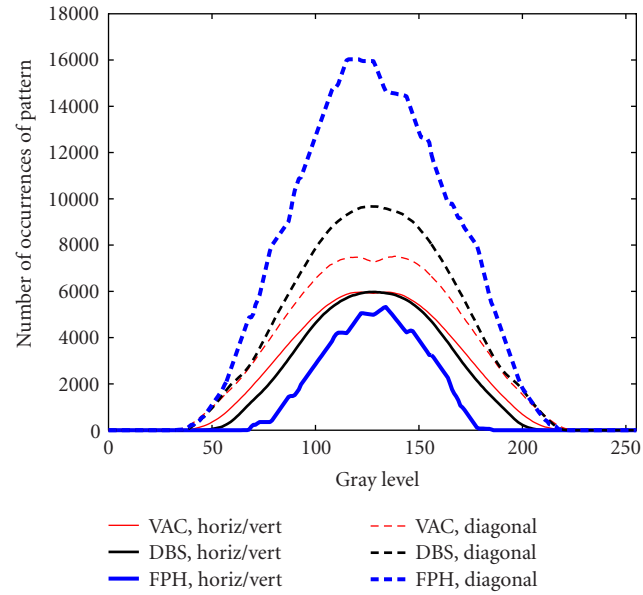

Figure 15: Morphological characterization of dot profiles of FPH (Λ_2) versus those of VAC and DBS: horizontal/vertical patterns versus diagonal patterns.

ACKNOWLEDGMENTS

This research has been supported in part by a Grant from the Natural Sciences and Engineering Research Council (NSERC) of Canada. The authors acknowledge with thanks the help of Sang Ho Kim and Jan P. Allebach in preparing the halftones using dual-metric direct binary search screens and the calculation of the quantitative halftone quality measures on these masks.

REFERENCES

[1] M. Yao and K. Parker, "Modified approach to the construction of a blue noise mask," *Journal of Electronic Imaging*, vol. 3, no. 1, pp. 92–97, 1994.

[2] R. A. Ulichney, "Void-and-cluster method for dither array generation," in *Human Vision, Visual Processing, and Digital Display IV*, J. P. Allebach and B. E. Rogowitz, Eds., vol. 1913 of *Proceedings of SPIE*, pp. 332–343, San Jose, Calif, USA, February 1993.

[3] J. Allebach and Q. Lin, "FM screen design using DBS algorithm," in *Proc. IEEE International Conference on Image Processing (ICIP '96)*, vol. 1, pp. 549–552, Lausanne, Switzerland, September 1996.

[4] D. Kacker and J. P. Allebach, "Aperiodic microscreen design using DBS and training," in *Color Imaging: Device-Independent Color, Color Hardcopy, and Graphic Arts III*, G. B. Beretta and R. Eschbach, Eds., vol. 3300 of *Proceedings of SPIE*, pp. 386–397, San Jose, Calif, USA, January 1998.

[5] P. Li and J. P. Allebach, "Look-up-table based halftoning algorithm," *IEEE Trans. Image Processing*, vol. 9, no. 9, pp. 1593–1603, 2000.

[6] S. H. Kim and J. P. Allebach, "Impact of HVS models on model-based halftoning," *IEEE Trans. Image Processing*, vol. 11, no. 3, pp. 258–269, 2002.

[7] P. G. Anderson, "Error diffusion using linear pixel shuffling," in *Proc. Image Processing, Image Quality, Image Capture Systems Conference (PICS '00)*, pp. 231–235, Portland, Ore, USA, March 2000.

[8] H. R. Kang, *Digital Color Halftoning*, SPIE Optical Engineering Press, Bellingham, Wash, USA, 1999.

[9] Y. Eldar, M. Lindenbaum, M. Porat, and Y. Y. Zeevi, "The farthest point strategy for progressive image sampling," *IEEE Trans. Image Processing*, vol. 6, no. 9, pp. 1305–1315, 1997.

[10] R. A. Ulichney, "Dithering with blue noise," *Proceedings of the IEEE*, vol. 76, no. 1, pp. 56–79, 1988.

[11] R. Shahidi, C. Moloney, and G. Ramponi, "Farthest point halftoning," in *Proc. IEEE-EURASIP Workshop on Nonlinear Signal and Image Processing (NSIP '03)*, Grado, Italy, June 2003.

[12] T. Scheermesser and O. Bryngdahl, "Spatially dependent texture analysis and control in digital halftoning," *Journal of the Optical Society of America A*, vol. 14, no. 4, pp. 827–835, 1997.

[13] B. L. Evans, V. Monga, and N. Damera-Venkata, "Halftoning toolbox for MATLAB," version 1.1, November 2002, http://www.ece.utexas.edu/~bevans/projects/halftoning/.

[14] P. W. Wong, "Entropy-constrained halftoning using multipath tree coding," *IEEE Trans. Image Processing*, vol. 6, no. 11, pp. 1567–1579, 1997.

[15] V. Misic and K. J. Parker, "Morphological characterization of dithering masks," *Journal of Electronic Imaging*, vol. 12, no. 2, pp. 278–283, 2003.

[16] M. Yao, *Blue noise halftoning*, Ph.D. thesis, University of Rochester, Rochester, NY, USA, 1996.

R. Shahidi was born in Montreal, Canada, in 1977. He graduated with a Joint Honours Pure Mathematics and Computer Science B. Math degree from the University of Waterloo, Canada, in 1999. Mr. Shahidi was awarded an M. Eng. degree from Memorial University of Newfoundland, Canada, in 2003, and is currently pursuing a Ph.D. in engineering also from Memorial University of Newfoundland in the field of nonlinear PDE models for image processing. His research interests include image processing, image analysis, and software engineering.

C. Moloney received the B.S. (with honours) degree in mathematics from Memorial University of Newfoundland, Canada, and the M.A.S. and Ph.D. degrees in systems design engineering from the University of Waterloo, Canada. Since 1990, she has been a faculty member with Memorial University of Newfoundland, where she is now a Professor of electrical and computer engineering. Her research interests include nonlinear image processing, SAR image processing and applications, and digital signal processing of musical and other acoustic signals.

G. Ramponi was born in Trieste, Italy, in 1956. He received the degree in electronic engineering (with highest honours) in 1981; he has been a Researcher then an Associate Professor, and since 2000, he is a Full Professor of electronics at the Department of Electronics, University of Trieste. His research interests include nonlinear digital signal processing, enhancement and feature extraction in images and image sequences, and image compression. He is the coinventor of various pending international patents and has published more than 120 papers in international journals, conference proceedings, and book chapters. Professor Ramponi was an Associate Editor of the IEEE Signal Processing Letters and is presently an Associate Editor of the IEEE Transactions on Image Processing and of the SPIE Journal of Electronic Imaging. He was Chairman of the Technical Programme of NSIP-03 and of Eusipco-96. He has been the local representative responsible for various scientific activities and contracts both at the European level (LTR, ESPRIT, TMR) and at the national level (CNR, MIUR), and has participated in other European and national research projects.